Published in final edited form as:
Science. 2008 October 24; 322(5901): 597–602. doi:10.1126/science.1162790.

Functional Targeting of DNA Damage to a Nuclear Pore–Associated SUMO-Dependent Ubiquitin Ligase

Shigeki Nagai[1,2,*], **Karine Dubrana**[2,*,†], **Monika Tsai-Pflugfelder**[1], **Marta B. Davidson**[3], **Tania M. Roberts**[3], **Grant W. Brown**[3], **Elisa Varela**[1], **Florence Hediger**[2], **Susan M. Gasser**[1,2,‡], and **Nevan J. Krogan**[4]

[1]Friedrich Miescher Institute for Biomedical Research, Maulbeerstrasse 66, 4058 Basel, Switzerland [2]Department of Molecular Biology and National Center of Competence in Research Frontiers in Genetics, 30 Quai Ernest Ansermet, 1211 Geneva, Switzerland [3]Department of Biochemistry, Donnelly Centre for Cellular and Biomolecular Research, University of Toronto, 160 College Street, Toronto, Ontario M5S 3E1, Canada [4]Department of Cellular and Molecular Pharmacology, California Institute for Quantitative Biomedical Research, University of California, San Francisco, 1700 Fourth Street, San Francisco, CA 94158, USA

Abstract

Recent findings suggest important roles for nuclear organization in gene expression. In contrast, little is known about how nuclear organization contributes to genome stability. Epistasis analysis (E-MAP) using DNA repair factors in yeast indicated a functional relationship between a nuclear pore subcomplex and Slx5/Slx8, a small ubiquitin-like modifier (SUMO)–dependent ubiquitin ligase, which we show physically interact. Real-time imaging and chromatin immunoprecipitation confirmed stable recruitment of damaged DNA to nuclear pores. Relocation required the Nup84 complex and Mec1/Tel1 kinases. Spontaneous gene conversion can be enhanced in a Slx8- and Nup84-dependent manner by tethering donor sites at the nuclear periphery. This suggests that strand breaks are shunted to nuclear pores for a repair pathway controlled by a conserved SUMO-dependent E3 ligase.

Nuclear pores have been implicated in a range of cellular processes, including macromolecular transport, transcription, and DNA repair. Recent work in several species argues that the binding of genes at nuclear pores contributes to transcriptional regulation (1, 2). At the same time, mutations in components of a pore subcomplex (Nup84, Nup120, Nup133, and Nup60) rendered yeast cells hypersensitive to DNA damaging agents (3–5). Moreover, the loss of yeast telomere anchoring reduced DNA repair selectively in subtelomeric regions (3), and loss of the Nup84 complex was shown to be synthetic lethal with mutations that impair homologous recombination (5, 6). Such strains accumulated spontaneous damage (5, 7), a phenotype partially suppressed by overexpression of a pore-associated desumoylating enzyme, Ulp1 (7, 8). Although Ulp1 is an essential enzyme whose

‡To whom correspondence should be addressed. susan.gasser@fmi.ch.
*These authors contributed equally to this work.
†Present address: UMR218, Institut Curie/Section de Recherche, 26 Rue d'Ulm, 75231 Paris, and Institut de Radiobiologie Cellulaire et Moléculaire, CEA, 92265 Fontenay aux Roses, France.

Supporting Online Material
www.sciencemag.org/cgi/content/full/322/5901/597/DC1
Materials and Methods
Figs. S1 to S7
Table S1
References

loss also impairs transport through nuclear pores (9), it was suggested that nuclear pores and SUMO metabolism might contribute to DNA repair.

To examine this further, we mapped the subnuclear position and dynamics of a tagged DNA double strand break (DSB) in vivo by using the yeast strain JKM179 (10). In this strain, a single cut can be induced at the mating type locus (*MAT*) by galactose-controlled expression of the HO endonuclease (11). To a strain lacking donor sequences for homologous recombination (HR), we added lacI binding sites (256×lacO) adjacent to *MAT*. Expressing a green fluorescent protein (GFP)–lacI fusion protein enabled tracking of the DSB by live fluorescence microscopy with respect to the nuclear envelope (NE), visualized through a Nup49-GFP fusion (12) (Fig. 1A).

To determine the subnuclear localization of a DSB at *MAT*, we acquired 18-step stacks of images of yeast cells growing in agar (Fig. 1B) and scored the position of the GFP-tagged DSB relative to the nearest pore signal. This value was divided by the nuclear diameter in the plane of focus, and ratios were binned into three concentric zones of equal surface, such that a random distribution yields 33% per zone (12).

In the absence of HO-induced cleavage (growth in glucose), GFP-*MAT* was randomly distributed throughout the nuclei (Fig. 1C). Yet 2 hours after HO induction, the cleaved *MAT* locus was enriched in the outermost zone (56%; $P = 7.6 \times 10^{-8}$) (Fig. 1C). The *mat*a^{ho} locus, bearing an uncleavable HO consensus (Fig. 1C) or unrelated tagged loci (e.g., ARS607; fig. S1) showed no redistribution upon galactose-induced expression of HO.

The relocalization of the HO-induced DSB to the NE was not immediate, occurring between 0.5 and 2 hours after cut induction (fig. S1A), yet it persisted for over 4 hours. The DSB was also readily detected at the NE by immunostaining for ATR kinase, Mec1 (13) (fig. S2, A and B). Importantly, when donor sequences for repair of the DSB by HR were present, *MAT* remained randomly distributed despite HO induction (Fig. 1C and fig. S1B).

Live time-lapse imaging of the uncut *MAT* locus shows subdiffusive movement within a radius of about 0.6 μm (14). This movement was unchanged after 30 min of HO-endonuclease induction, although by 2 hours the cut site showed highly constrained movement (Fig. 1D). We quantify increased constraint by scoring the frequency of large steps [>0.5 μm/1.5 s (14)] and radial movement (fig. S1C). Sequestration at the NE correlated temporally with resection of the DSB and accumulation of Mec1/Ddc2 (13) but not with the recruitment of yKu, Rad52, or Mre11 complex (15). Importantly, the DSB did not colocalize with telomere clusters at the NE (fig. S2C).

In unperturbed S-phase cells, foci of checkpoint and repair proteins form at spontaneous DNA breaks that arise from dysfunctional replication forks (16). Prolonged incubation in hydroxyurea (HU) enhanced the appearance of such foci, as did pretreatment of cells with methylmethane sulfonate (MMS), an alkylating agent that induces nicks (17) (fig. S3A). Because DNA polymerases remain fork-associated and able to restart for ~1 hour on HU (18), we could ask whether this stalling of polymerases or fork collapse itself provoked the relocation of the lacOtagged origin ARS607 to the NE (Fig. 2A). In an unsynchronized yeast culture exposed to 0.2 M HU, we could track a shift from random to perinuclear positioning only after prolonged HU treatment [50% zone 1 at 2 hours, $P = 8 \times 10^{-5}$ (Fig. 2B)]. Furthermore, when cells were synchronously released from G1 phase into HU for 1 hour, allowing polymerases to stall, ARS607 remained randomly distributed unless fork breakage was enhanced by treating cells additionally with MMS (Fig. 2C). A late-firing origin (ARS1412) that does not fire under these conditions did not shift (Fig. 2C), nor did origins in cells treated with MMS alone (fig. S1A). We thus conclude that fork-associated breaks, rather than polymerase pausing, triggers relocation to the NE.

To see whether the collapsed forks colocalized with nuclear pores, we introduced an N-terminal deletion of Nup133 [*nup133*ΔN (19)] in a strain expressing cyan fluorescent protein (CFP)–Nup49. In this mutant, pores cluster on one side of the nucleus, yet DNA repair and mRNA export are unperturbed (5, 19). In HU and MMS, colocalization of GFP-tagged ARS607 with the clustered CFP-pore signal doubled (Fig. 2D), suggesting that collapsed replication forks may interact with pores.

Further insight into the damage–nuclear pore connection arose from an E-MAP (epistatic-miniarray profile) analysis (20), which compiled both negative (e.g., synthetic lethality) and positive (e.g., suppression) interactions between 743 genes involved in nuclear function (21). Whereas individual interactions can be difficult to interpret, hierarchical clustering allows the grouping of functionally related genes according to the similarity of their interaction profiles (20, 21). Three nonessential components of the Nup84 nuclear pore complex, *NUP60, NUP84*, and *NUP133*, clustered with factors involved in DNA replication and repair, whereas genes for other pore factors, notably Nup82, Nup192, and Nup157, did not.

Intriguingly, deletions of Nup84 complex genes behaved most similarly to deletions of *SLX5* and *SLX8*, genes encoding a heterodimeric complex implicated in DNA repair (Fig. 3, A and B). Slx5 harbors two small ubiquitin-like modifier (SUMO) recognition motifs, and Slx8 bears a RING domain with ubiquitin ligase activity (22–28). This complex directly binds DNA (27), and deletion of either gene leads to an accumulation of sumoylated proteins (26). Despite the striking similarity of Slx5 and Slx8 genetic profiles with those of the Nup84 complex, double deletions of *slx5* or *slx8* with *nup84* or *nup60* display negative interactions (Fig. 3A). This suggests that, despite their functional relatedness, their contributions to cell survival do not entirely overlap.

We next tested whether Slx5 and Slx8 colocalize with nuclear pores by double immunostaining for hemagglutinin (HA)–tagged Slx5 or Slx8 and pores. Deconvolution confocal microscopy showed a considerable degree of coincidence of the two signals at the nuclear rim, although anti-Slx5/8 also labels speckles throughout the nucleoplasm (Fig. 3C) (24). The overlap of Slx8-HA with nuclear pores was not enhanced by treating cells with zeocin, which induces DSB by chemical insult (fig. S3).

To test whether Slx5 and Slx8 are physically associated with pore complexes, we Myc-tagged Nup84 in strains bearing HA-tagged Slx5 or Slx8 and monitored interaction by reciprocal coimmunoprecipitation. We detected a robust coprecipitation of HA-tagged Slx8 with anti-Myc only in cells bearing the Nup84-Myc fusion (Fig. 3D). Reciprocally, Nup84-Myc was recovered in an anti–Slx8-HA precipitate (Fig. 3D). Neither DNA damage nor formaldehyde fixation altered the efficiency of their interaction (fig. S4), arguing that Nup84 and the Slx5/Slx8 complex interact (22, 23, 27, 28).

It remained to be seen whether nuclear pore proteins and/or Slx5/Slx8 associate with an irreparable DSB when it moves to the NE. Chromatin immunoprecipitation (ChIP) on cross-linked then sonicated yeast cells was first performed with a monoclonal antibody (Mab414) that recognizes FG repeat–containing pore components. Indeed, after a 2-hour HO induction, we found significant and selective recovery of *MAT* with pore proteins in a cleavage-dependent manner (fig. S5).

With use of Myc-tagged versions of Nup84 and Nup133, we then monitored the DSB association of the Slx5/Slx8-associated nuclear pore proteins. Both nucleoporins became closely associated with the DSB, peaking 2 to 4 hours after HO induction (Fig. 4, B and C). No enrichment was observed in strains lacking the HO endonuclease or the epitope tag, confirming the association is damage-specific. Pore association of the DSB required an

intact Nup84 complex because the DSB-Nup84 interaction was compromised in *NUP120* or *NUP133* deletion strains (Fig. 4C), consistent with these mutants' hypersensitivity to DNA damage (4, 5). We further confirmed that Slx8 binds directly to a DSB by performing ChIP with Slx8-Myc (Fig. 4D). Together with the imaging results, we conclude that DSB association with nuclear pores requires intact Nup84 complex.

The kinetics of the perinuclear shift suggested that end-processing might influence the relocalization of damage. Potential regulators include Mec1/Tel1, the ATR/ATM checkpoint kinases in budding yeast, which are recruited to DSBs to trigger repair and delay cell cycle progression (13). Moreover, Mec1-Ddc2 accumulate at resected DSBs with kinetics similar to that of DSB-pore association (13). To test whether Mec1 or Tel1 is needed for damage relocalization, we performed Nup84-Myc ChIP in strains lacking Mec1 and/or Tel1, each combined with *sml1*Δ to ensure viability. Whereas the recruitment of Nup84-Myc to *MAT* was only slightly impaired in *mec1sml1* strain, loss of both kinases abolished the association (Fig. 4E).

The effect of Mec1 kinase activity on DSB localization was also monitored by live microscopy of the lacO-tagged HO cut in the *mec1*-kinase dead background (13) (Fig. 4F). Relocation of the cleaved *MAT* locus was reduced by *mec1*mutation but was not dependent on the downstream checkpoint response. We detected robust relocation of GFP-tagged *MAT* locus in a *rad9*Δ mutant (Fig. 4F). Importantly, loss of yKu or deletion of genes encoding two pore-associated proteins, Mlp1 and Mlp2, had no effect on DSB relocalization (Fig. 4F). Because Ulp1 protein levels drop dramatically in the *mlp1/2* double mutant (7, 8), it is unlikely that Ulp1 is involved in damage relocalization, although it is possible that Ulp1 regulates downstream repair events. Given that Ulp1 is implicated in the maintenance of genome stability (7, 29) and *slx5/slx8* mutants are synthetically sick with a temperature-sensitive *ulp1* allele (23), Slx5/Slx8 may function in parallel to Ulp1.

Further support for a role of Nup84, Slx5, and Slx8 in DNA repair is the significant increase in spontaneous foci of the recombination protein Rad52 or the Mec1 cofactor, Ddc2, in *slx5/8* mutants (Fig. 5A) (5, 24, 25). We also detect enhanced rates of spontaneous gross chromosomal rearrangement (GCR) (Fig. 5B) (25). Lastly, both *nup84* and *nup120* deletion strains fail to efficiently restart replication after prolonged arrest on combinations of HU and MMS (fig. S6). We propose that the Nup84-Slx5/8 complex resolves DNA damage at collapsed forks, leading to the reduced accumulation of damage foci and suppression of inappropriate genomic rearrangements.

Spontaneous gene conversion (GC) events are thought to arise from damage at replication forks. To score these, we exploited a repair system in which heteroallelic mutations in the *lys2* gene are placed on nonhomologous chromosomes. Restoration of a functional *LYS2* gene requires spontaneous GC (30), an event allowing for growth without lysine (Fig. 5C). We found that loss of Nup84 or Slx8 leads to a dramatic increase in spontaneous GC events, which is suppressed by plasmid-borne wild-type *NUP84* or *SLX8* (Fig. 5D). This is consistentwith increased rates of fork-associated damage in these mutants.

To examine whether artificial recruitment of a locus near nuclear pores enhances GC in a wild-type background, we added four lexA binding sites upstream of the *lys2* allele on ChrII and introduced NE-associated proteins LexA-Yif1 or LexA-Nup84 (Fig. 5C). The binding of such fusion proteins shifts the internal locus to the nuclear periphery (fig. S7). The impact of relocalization on GC was then tested by monitoring rates of spontaneous Lys+ colony formation. We found six fold higher GC rates in the presence of either LexA-Nup84 or LexA-Yif1 compared with LexA (Fig. 5D). This was not associated with loss of viability or

altered cell division, although the increase in GC conferred by the perinuclear anchor could reflect either increased damage or increased repair.

To resolve this, we asked whether the enhancement of GC achieved by anchoring required the Nup84-Slx5/Slx8 complex. We monitored GC rates with tethered donor loci in *slx8*Δ or *nup84*Δ and found that the increased GC rate conferred by tethering was lost in the mutants (Fig. 5, D and E). One simple interpretation is that the absence of Slx8 or Nup84 attenuates a repair pathway that requires anchorage at or near nuclear pores.

These data support a functional role for the Nup84 complex as a coordinator of SUMO-dependent repair pathways. There is a remarkable selectivity in the recruitment for irreparable DSBs and collapsed replication forks because we score no shift of stalled replication forks or DSBs reparable by HR. This argues for a specific pathway of repair requiring both the Nup84 complex and the Slx5/Slx8 SUMO-dependent ubiquitin ligase. Given the hypersensitivity of *slx5* and *slx8* mutants to HU (22, 25), we propose that this pathway facilitates collapsed replication fork recovery. Although the translocation of damage to the NE does not require Slx5/Slx8, the enhanced rate of repair conferred by pore association does.

A sumoylated protein may accumulate at collapsed forks or irreparable DSBs, requiring Slx5/Slx8 ubiquinylation and proteasomal degradation to enable appropriate repair. The E-MAP data (Fig. 3A) and the fact that Slx5/Slx8 are physically associated with the proteasome (31) support this model (Fig. 5F). Furthermore, the presence of the proteasome at the NE (32) provides a rationale for the observed relocalization. Lastly, the proteasome is recruited to DSBs (33). Thus, we propose that the Slx5/Slx8 pathway involves targeted degradation of a sumoylated protein bound at collapsed forks or resected breaks (Fig. 5F). The relevant targets of Slx5/Slx8 ubiquitination are unknown, but likely candidates based on E-MAP data include Pol32, Rad27, and Srs2 (Fig. 3) (21).

Supplementary Material

Refer to Web version on PubMed Central for supplementary material.

Acknowledgments

We thank J. E. Haber, M. Lisby, S. Jinks-Robertson, R. Kolodner, and R. Rothstein for generously providing strains; M. Shales for artwork; K. Saeturn and V. Kalck for technical help; and C. J. Ingles, J. E. Haber, and our laboratories for discussions. We acknowledge the Novartis Research Foundation, Swiss Cancer League, Swiss National Science Foundation, Sandler Family Foundation, NIH, National Cancer Institute of Canada, and Canadian Cancer Society for support.

References and Notes

1. Schneider R, Grosschedl R. Genes Dev. 2007; 21:3027. [PubMed: 18056419]
2. Akhtar A, Gasser SM. Nat. Rev. Genet. 2007; 8:507. [PubMed: 17549064]
3. Therizols P, et al. J. Cell Biol. 2006; 172:189. [PubMed: 16418532]
4. Bennett CB, et al. Nat. Genet. 2001; 29:426. [PubMed: 11726929]
5. Loeillet S, et al. DNA Repair. 2005; 4:459. [PubMed: 15725626]
6. Pan X, et al. Cell. 2006; 124:1069. [PubMed: 16487579]
7. Palancade B, et al. Mol. Biol. Cell. 2007; 18:2912. [PubMed: 17538013]
8. Zhao X, Wu CY, Blobel G. J. Cell Biol. 2004; 167:605. [PubMed: 15557117]
9. Stade K, et al. J. Biol. Chem. 2002; 277:49554. [PubMed: 12393908]
10. Materials and methods are available as supporting material on *Science* Online.
11. Lee SE, et al. Cell. 1998; 94:399. [PubMed: 9708741]

12. Hediger F, Taddei A, Neumann FR, Gasser SM. Methods Enzymol. 2004; 375:345. [PubMed: 14870677]
13. Dubrana K, van Attikum H, Hediger F, Gasser SM. J. Cell Sci. 2007; 120:4209. [PubMed: 18003698]
14. Heun P, Laroche T, Shimada K, Furrer P, Gasser SM. Science. 2001; 294:2181. [PubMed: 11739961]
15. Wang XH, Haber JE. PLoS Biol. 2004; 2:E21. [PubMed: 14737196]
16. Lisby M, Mortensen UH, Rothstein R. Nat. Cell Biol. 2003; 5:572. [PubMed: 12766777]
17. Tercero JA, Diffley JF. Nature. 2001; 412:553. [PubMed: 11484057]
18. Cobb JA, et al. Genes Dev. 2005; 19:3055. [PubMed: 16357221]
19. Doye V, Wepf R, Hurt EC. EMBO J. 1994; 13:6062. [PubMed: 7813444]
20. Schuldiner M, et al. Cell. 2005; 123:507. [PubMed: 16269340]
21. Collins SR, et al. Nature. 2007; 446:806. [PubMed: 17314980]
22. Mullen JR, Kaliraman V, Ibrahim SS, Brill SJ. Genetics. 2001; 157:103. [PubMed: 11139495]
23. Xie Y, et al. J. Biol. Chem. 2007; 282:34176. [PubMed: 17848550]
24. Burgess RC, Rahman S, Lisby M, Rothstein R, Zhao X. Mol. Cell. Biol. 2007; 27:6153. [PubMed: 17591698]
25. Zhang C, Roberts TM, Yang J, Desai R, Brown GW. DNA Repair. 2006; 5:336. [PubMed: 16325482]
26. Wang Z, Jones GM, Prelich G. Genetics. 2006; 172:1499. [PubMed: 16387868]
27. Yang L, Mullen JR, Brill SJ. Nucleic Acids Res. 2006; 34:5541. [PubMed: 17020915]
28. Prudden J, et al. EMBO J. 2007; 26:4089. [PubMed: 17762865]
29. Soustelle C, et al. Mol. Cell. Biol. 2004; 24:5130. [PubMed: 15169880]
30. Freedman JA, Jinks-Robertson S. Genetics. 2002; 162:15. [PubMed: 12242220]
31. Collins SR, et al. Mol. Cell. Proteomics. 2007; 6:439. [PubMed: 17200106]
32. Enenkel C, Lehmann A, Kloetzel PM. Mol. Biol. Rep. 1999; 26:131. [PubMed: 10363659]
33. Krogan N, et al. Mol. Cell. 2004; 16:1027. [PubMed: 15610744]

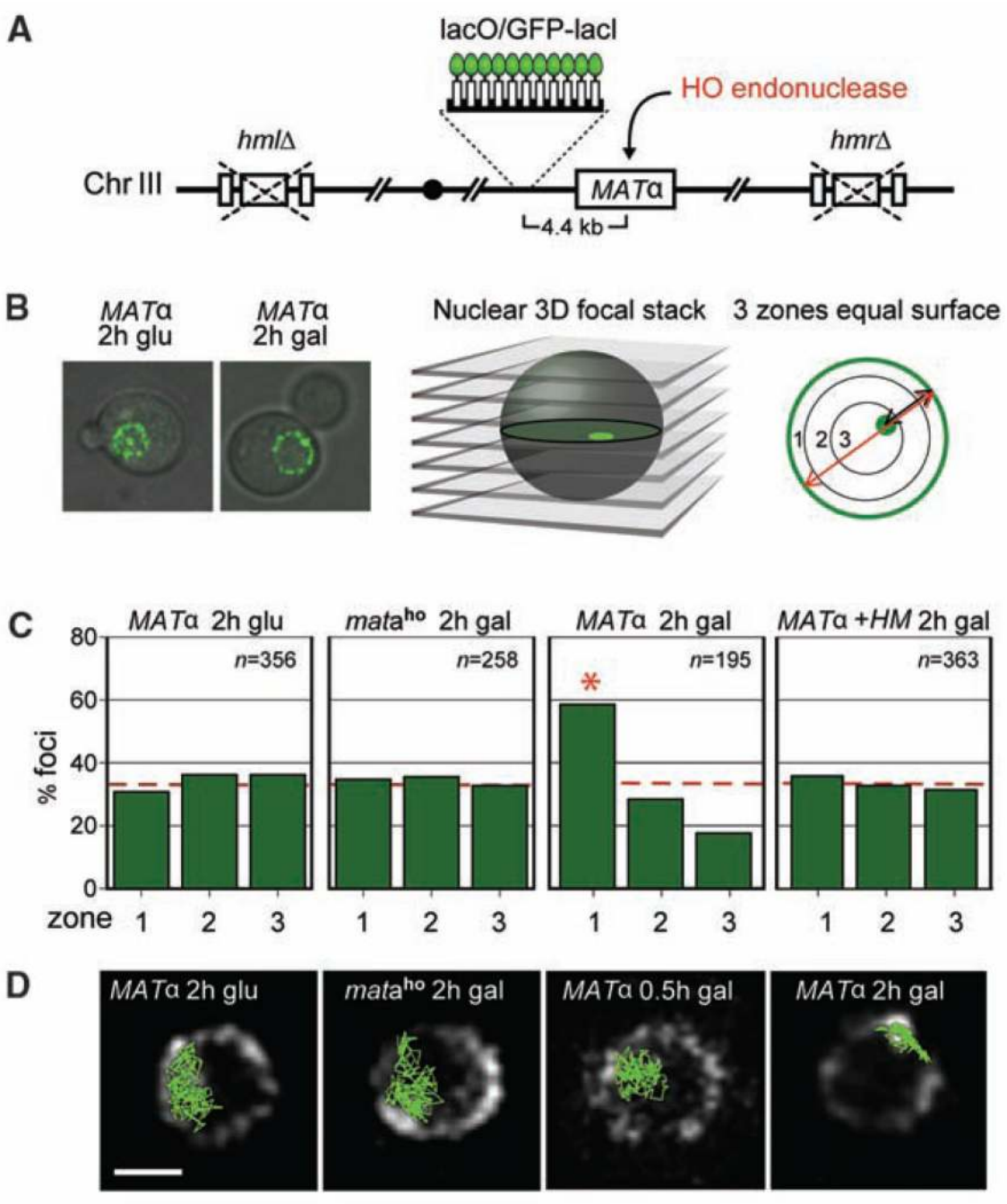

Fig. 1.

Relocation of an irreparable DSB to the nuclear periphery. (**A**) Galactose induces a DSB at *MAT* in a haploid strain that lacks homologous donor loci (11), bears lacO sites 4.4 kb from *MAT*α, and expresses GFP-lacI and Nup49-GFP fusion proteins (GA-1496). (**B**) Position of the GFP-tagged *MAT* locus was scored relative to the NE (single-plane confocal images detecting Nup49 and *MAT* signals). Ratios of distance from NE and diameter in focal plane are binned into equal concentric zones (12). (**C**) Results of scoring *MAT* position in GA-1496 or in strains with either an uncleavable HO site (*mata*^{ho}, GA-1965) or *HM* loci (*HML HMR*; GA-2269). Red bar indicates random distribution, and an asterisk indicates

significantly nonrandom. Number of cells analyzed and confidence values for a proportional test between random and experimental distribution are (for *MAT*α and 2-hours glucose, 356 and $P = 1.6 \times 10^{-1}$; for *mat*a^{ho} 2-hours galactose, 258 and $P = 8.9 \times 10^{-1}$; *MAT*α 2-hours galactose, 195 and $P = 4.5 \times 10^{-8}$; and *MAT*α+*HM*, 363 and $P = 3.2 \times 10^{-1}$). (**D**) 250 sequential confocal frames at 1.5-s intervals were aligned by the pore signals for G1 phase cells of the strains used in (C) (12), and *MAT* position was marked in each frame. Five-min trajectories are green. Bar indicates 1 μm.

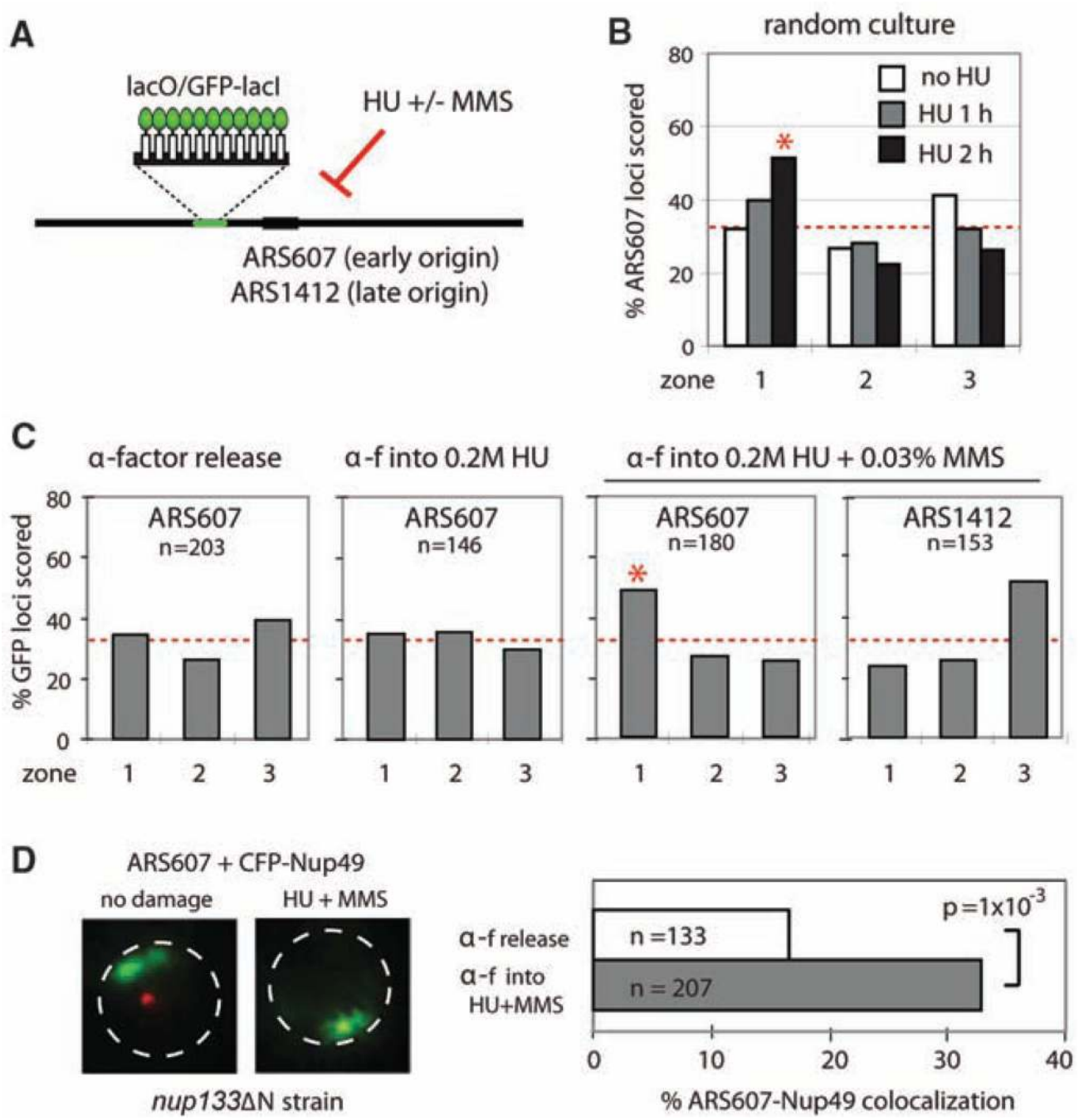

Fig. 2.

Collapsed replication forks colocalize with pores. (**A**) Position of LacO-tagged early origin ARS607 (GA-1461) or late origin ARS1412 (GA-2070) was determined as in Fig. 1. (**B**) Exponentially growing GA-1461 cells were incubated ±0.2 M HU 1 or 2 hours. Spot position in S-phase cells was scored as in Fig. 1. Zone 1 enrichment by 2 hours is significant ($P = 8 \times 10^{-5}$). (**C**) Strains as in (A) were synchronized in G1 by α-factor treatment and released into 0.2 M HU ± 0.033% MMS for 1 hour. Zone 1 enrichment of collapsed forks is significant (asterisk indicates $P = 2 \times 10^{-5}$). (**D**) GFP-tagged ARS607 (red) and a CFP-Nup49 fusion (green) were expressed in a *nup133*Δ background expressing nup133Δ 44–

236 (19). Cells synchronized in G1 phase were released 1 hour in 0.033% MMS plus 0.2 M HU. Deconvolved confocal sections of nuclei were scored for complete GFP-CFP signal overlap.

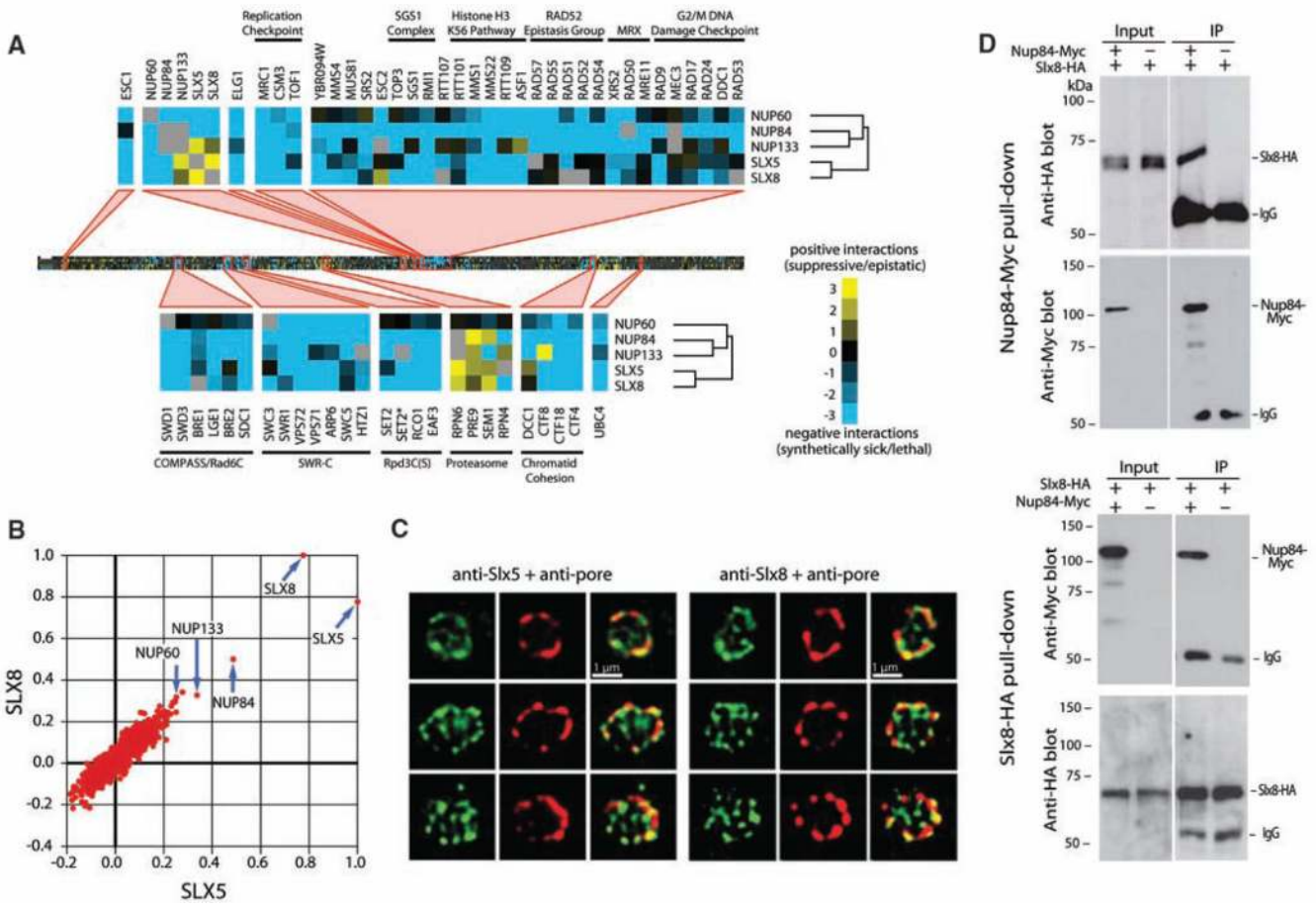

Fig. 3.

Nup84 complex and Slx5/Slx8 interact. (**A**) Hierarchical clustering of the nuclear function E-MAP (21). Genetic interactions from this map common to *nup60*Δ, *nup84*Δ, *nup133*Δ, *slx5*Δ, and *slx8*Δ are highlighted in blue and yellow. (**B**) Plot of correlation coefficients generated from comparison of the genetic profiles from *slx5*Δ or *slx8*Δ to all other profiles in this E-MAP. (**C**) Rat anti-HA (in green) and mouse anti–nuclear pore (Mab414, in red) colocalized by deconvolved confocal imaging of cells bearing Slx5-HA (GA-3867) or Slx8-HA (GA-3868). (**D**) Coimmunoprecipitation of Slx8 with Nup84 from cells bearing both Slx8-HA and Nup84-Myc (GA-5161) or Slx8-HA alone (GA-3868) (10). Westerns of proteins recovered with anti-Myc– or anti-HA–coated magnetic beads were probed with both antibodies. IgG, immunoglobulin G.

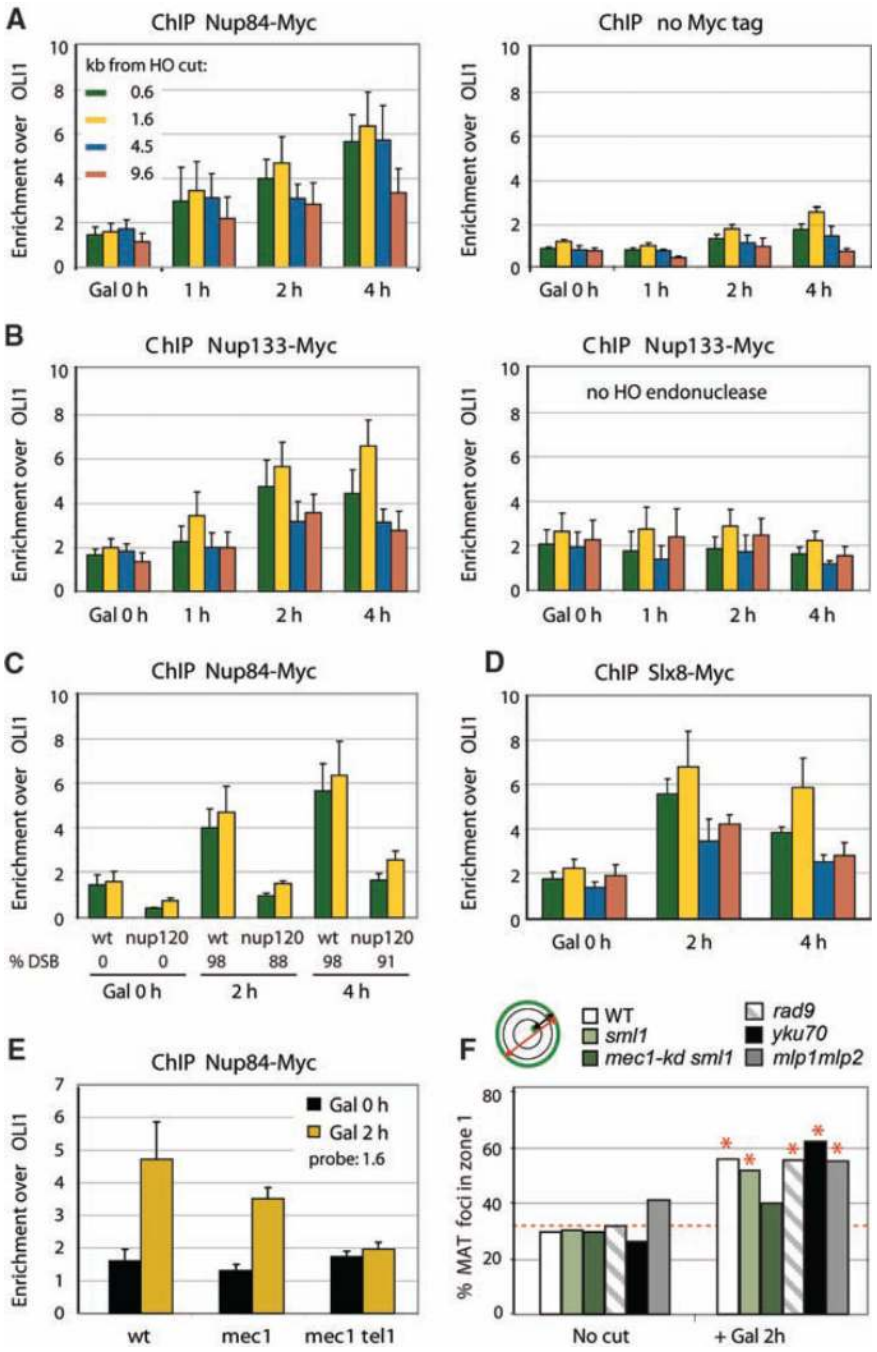

Fig. 4.

An irreparable DSB interacts with nuclear pores. (**A** and **B**) ChIP with anti-Myc in JKM179 derivatives with or without Nup84-Myc (GA-4133) or Nup133-Myc, with or without *GAL1:*HO (GA-4135 and GA-4140) at indicated time points on galactose. Primer/probe sets for real-time polymerase chain reaction are 0.6 kb, 1.6 kb, 4.5 kb, and 9.6 kb from the HO cut. For calculation of absolute enrichment over a mitochondrial gene, *OLI1*, see (10). (**C**) Anti–Nup84-Myc ChIP in a *nup120*Δ mutant (GA-4861) and a wild-type strain, as in (A). (**D**) Anti-Myc ChIP for Slx8-13Myc in GA-4137, as in (A). (**E**) ChIP for Nup84-Myc was performed in *mec1*Δ*sml1*Δ (GA-4847), *mec*1Δ*tel1*Δ *sml1*Δ, or wild-type strains. Absolute

enrichment of *MAT*+1.6 kb over *OLI1* as in (A). (**F**) The position of cleaved *MAT* was scored as in Fig. 1B in isogenic strains ± 2 hour HO induction. Strains and *n* and *P* values are as follows: WT (GA-1496) no cut: 365, 1.6×10^{-1}; cut: 195, 4.5×10^{-8}; *yku70* (GA-1954) no cut: 118, 6.8×10^{-2}; cut: 117, 2.6×10^{-11}; *mlp1mlp2* (GA-2228) no cut: 174, 3.7×10^{-2}; cut: 184, 5.5×10^{-10}: 148, 5.6×10^{-1}; *mec1-kd1 sml1* (13) (GA-2488) no cut: 269, 5.8×10^{-2}; cut: 228, 9.2×10^{-2}; *sml1*(13) (GA-2490) no cut: 205, 6.2×10^{-1}, cut: 151, 1.7×10^{-8}; *rad9* (GA-580) no cut: 315, 2.3×10^{-1}; cut: 309, 3.2×10^{-11}.

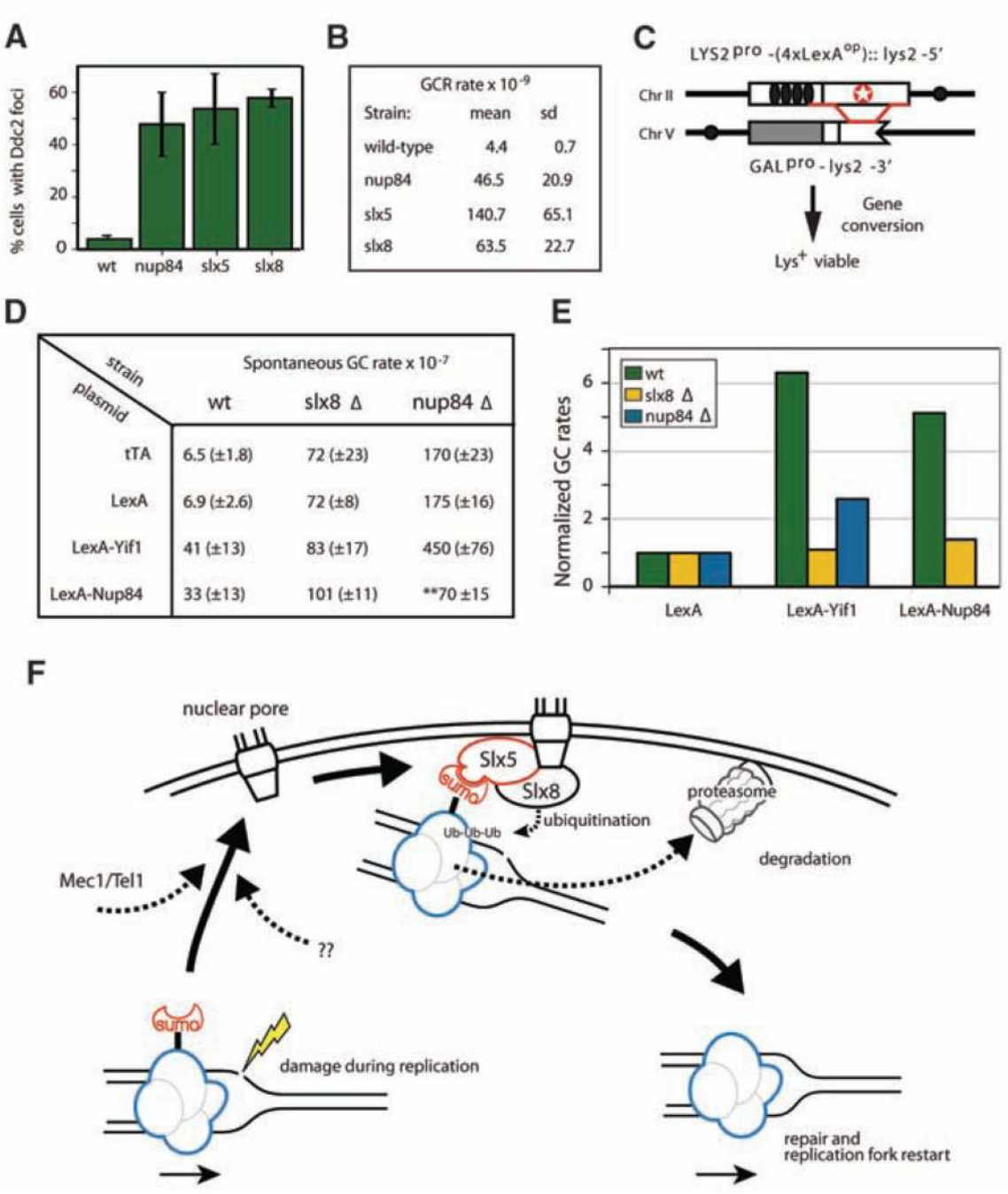

Fig. 5.

Slx5/Slx8-Nup84 complex mutants affect recombination and GC rates. (**A**) Percentage cells (n > 200) containing Ddc2–yellow fluorescent protein (YFP) foci in strains carrying indicated gene deletions; averaging and standard deviation over three experiments. (**B**) GCR rates (18) are enhanced in *nup84*Δ and *slx5*Δ or *slx8*Δ strains; averaging and standard deviations from three fluctuation tests. (**C**) Recombination substrates for GC assays on nonhomologous chromosomes were modified by integrating four LexA sites upstream of the *lys2* frameshift allele (white star;4lexA:*lys2*). ChrV carries 3′ truncated *lys2* allele. GC renders cells Lys+. (**D**) Perinuclear anchoring of 4lexA: *lys2* is achieved by expression of

fusions LexA-Yif1 or LexA-Nup84 (fig. S7). Spontaneous GC rates in wild-type or indicated mutants as in (30) and (10). Double asterisks indicate suppression of *slx8*Δ-enhanced GC rate by LexA-Slx8 expression. (**E**) Rates of GC in (D) were normalized to +LexA values. (**F**) Model of Mec1/Tel1-dependent relocation of damage to Nup84/Slx5/Slx8 complexes that may ubiquinylate a substrate for proteolysis, enabling fork-associated repair.